

RESEARCH PAPER

The T-type calcium channel antagonist, Z944, reduces spinal excitability and pain hypersensitivity

Erika K. Harding^{1,2,3}  | Annemarie Dedek^{4,5}  | Robert P. Bonin^{2,6}  |
 Michael W. Salter^{3,7}  | Terrance P. Snutch^{8,9}  | Michael E. Hildebrand^{4,5} 

¹Department of Comparative Biology and Experimental Medicine, University of Calgary, Calgary, Alberta, Canada

²Department of Pharmaceutical Sciences, Leslie Dan Faculty of Pharmacy, University of Toronto, Toronto, Ontario, Canada

³Program in Neurosciences and Mental Health, The Hospital for Sick Children, Toronto, Ontario, Canada

⁴Department of Neuroscience, Carleton University, Ottawa, Ontario, Canada

⁵Neuroscience Program, Ottawa Hospital Research Institute, Ottawa, Ontario, Canada

⁶University of Toronto Centre for the Study of Pain, University of Toronto, Toronto, Ontario, Canada

⁷Department of Physiology, University of Toronto, Toronto, Ontario, Canada

⁸Michael Smith Laboratories, University of British Columbia, Vancouver, British Columbia, Canada

⁹Djavad Mowafaghian Center for Brain Health, University of British Columbia, Vancouver, British Columbia, Canada

Correspondence

Michael E. Hildebrand, Department of Neuroscience, Carleton University, Ottawa, Ontario, Canada.
 Email: mike.hildebrand@carleton.ca

Funding information

Institute of Neurosciences, Mental Health and Addiction, Grant/Award Numbers: Operating Grant/ 10677, Operating Grant/ 154336; Natural Sciences and Engineering Research Council of Canada, Grant/Award Numbers: Discovery Grant/CU#315915, Industrial R&D Fellowship, CU#315915; Canadian Institutes

Background and Purpose: T-type voltage-gated calcium channels are an emerging therapeutic target for neurological disorders including epilepsy and pain. Inhibition of T-type channels reduces the excitability of peripheral nociceptive sensory neurons and reverses pain hypersensitivity in male rodent pain models. However, administration of peripherally restricted T-type antagonists failed to show efficacy in multiple clinical and preclinical pain trials, suggesting that inhibition of peripheral T-type channels alone may be insufficient for pain relief.

Experimental Approach: We utilized the selective and CNS-penetrant T-type channel antagonist, Z944, in electrophysiological, calcium imaging and behavioural paradigms to determine its effect on lamina I neuron excitability and inflammatory pain behaviours.

Key Results: Voltage-clamp recordings from lamina I spinal neurons of adult rats revealed that approximately 80% of neurons possess a low threshold T-type current, which was blocked by Z944. Due to this highly prevalent T-type current, Z944 potentially blocked action-potential evoked somatic and dendritic calcium transients in lamina I neurons. Moreover, application of Z944 to spinal cord slices attenuated action potential firing rates in over half of laminae I/II neurons. Finally, we found that intraperitoneal injection of Z944 (1–10 mg·kg⁻¹) dose-dependently reversed mechanical allodynia in the complete Freund's adjuvant model of persistent inflammatory pain, with a similar magnitude and time course of analgesic effects between male and female rats.

Conclusion and Implications: T-type calcium channels critically shape the excitability of lamina I pain processing neurons and inhibition of these channels by the clinical stage antagonist Z944 potentially reverses pain hypersensitivity across sexes.

KEYWORDS

calcium channels, dorsal horn, inflammatory pain, lamina I, neuronal excitability, Z944

Abbreviations: CFA, complete Freund's adjuvant; DRG, dorsal root ganglia; hERG, human ether-a-go-go-related gene.

Erika K. Harding and Annemarie Dedek contributed equally to this work.

This is an open access article under the terms of the Creative Commons Attribution-NonCommercial License, which permits use, distribution and reproduction in any medium, provided the original work is properly cited and is not used for commercial purposes.

© 2021 The Authors. *British Journal of Pharmacology* published by John Wiley & Sons Ltd on behalf of British Pharmacological Society.

of Health Research Institute of Neurosciences,
Mental Health and Addiction, Grant/Award
Numbers: 154336, 10677

1 | INTRODUCTION

T-type **voltage-gated calcium channels** are an important emerging molecular target for the treatment of pain (Bourinet et al., 2014; Todorovic & Jevtovic-Todorovic, 2011; Weiss & Zamponi, 2019). Given their unique gating kinetics and low voltage activation near resting membrane potentials, T-type channels regulate subthreshold excitability as well as action potential firing patterns in both physiological and pathological states (Cheong & Shin, 2013). For example, T-type currents promote low threshold spikes and rebound burst firing in subsets of thalamic neurons, which are implicated in both slow wave sleep oscillations as well as in absence seizures (Cain et al., 2018; Cain & Snutch, 2013; Cheong & Shin, 2013). Several anti-epileptic drugs including **ethosuximide** are thought to act in part through the inhibition of T-type channels (Weiss & Zamponi, 2019), and interestingly, these same T-type targeting clinical compounds have analgesic effects in rodents (Dogrul et al., 2003; Flatters & Bennett, 2004). More broadly, selective knockdown or block of T-type channels through genetic and pharmacological approaches reverses pain hypersensitivity in rodent models of pain including bladder pain (Tsubota et al., 2018), post-surgical pain (Joksimovic et al., 2019), inflammatory pain (Watanabe et al., 2015), nerve injury-induced pain (Bourinet et al., 2005; Feng et al., 2019) and chemotherapy-induced and diabetic peripheral neuropathies (Jacus et al., 2012; Li et al., 2017).

The involvement of T-type channels in mediating pain processing has been extensively studied in the periphery. Of the three T-type voltage-gated calcium channel subtypes, **Ca_v3.1**, **Ca_v3.2** and **Ca_v3.3**, the Ca_v3.2 isoform has been shown to be selectively upregulated within dorsal root ganglion (DRG) peripheral sensory neurons in rodent models of chronic pain (Fukami et al., 2017; García-Caballero et al., 2014; Gomez et al., 2020; Li et al., 2017; Watanabe et al., 2015). Interfering with the various pathological mechanisms that upregulate Ca_v3.2 in DRG neurons reverses pain hypersensitivity within these rodent models. In terms of subcellular localization, Ca_v3.2 channels are now known to be functionally expressed throughout DRG neurons, from nerve endings in skin hair follicles to the presynaptic terminals of primary afferents (François et al., 2015; Jacus et al., 2012). However, peripherally restricted T-type channel antagonists such as **ABT-639** have failed to show efficacy in multiple clinical pain trials (Serra et al., 2015; Wallace et al., 2016) as well as in some rodent studies (Picard et al., 2019). These findings raise the possibility that T-type channels within the spinal cord could be an important target for the treatment of pain.

The superficial dorsal horn of the spinal cord consists of lamina I and lamina II, which together receive the bulk of nociceptive information from the periphery and are highly involved in the processing and relay of nociceptive information to the brain (Bourinet et al., 2014; Todd, 2010). Although intrathecal spinal injections of

What is already known

- Administration of T-type calcium channel antagonists reverses hypersensitivity in male rodent models of pathological pain.

What does this study add

- T-type calcium channels are present in spinal lamina I neurons, shaping cellular and dendritic excitability.
- The T-type blocker, Z944, reverses pain hypersensitivity in both male and female rodents.

What is the clinical significance

- Our findings identify a novel central mechanism for Z944's potent reversal of pain hypersensitivity.
- Lack of sexual dimorphism in Z944's pain reversal is an important step towards clinical translation.

T-type antagonists reverse pain hypersensitivity in rodent pain models (Feng et al., 2019; Picard et al., 2019; Wen et al., 2010), the specific contributions of T-type channels to pain processing in the superficial dorsal horn are poorly understood. T-type mediated calcium currents have recently been found to be expressed in a subset (approximately 45 to 60%) of lamina II neurons of both mice and rats (Candelas et al., 2019; Wu et al., 2018). However, the potential contributions of T-type channels in regulating excitability within lamina I neuron subpopulations remain unexplored. This represents a significant knowledge gap given that lamina I contains the output projection neurons for the superficial dorsal horn nociceptive network (Todd, 2010) and hyperexcitability of lamina I neurons has been implicated in the development and maintenance of pathological pain (Ikeda et al., 2003; Keller et al., 2007; Liu et al., 2008).

The small organic compound, **Z944**, is a CNS-penetrant, high affinity T-type calcium channel antagonist originally under clinical development for the treatment of absence seizures (Tringham et al., 2012). Z944 selectively blocks T-type channels at nanomolar concentrations, with minimal effects on other voltage-gated calcium channels, cardiovascular-related hERG channels and **Na_v1.5** channels up to the low micromolar concentrations produced by systemic administration (Tringham et al., 2012). Cryo-electron microscopy has

demonstrated a direct physical interaction between Z944 and the central cavity of the T-type channel pore domain (Zhao et al., 2019). Recent evidence has suggested that Z944 has analgesic potential in both rodents and humans. In male rodents, systemic injection of Z944 alleviated behavioural measures of chronic neuropathic pain (Leblanc et al., 2016), while in human phase Ia and Ib clinical studies, both oral and systemic injection of Z944 were found to be well tolerated and reduced pain sensitization as well as Visual Analog Scale pain ratings in an experimental pain model (Lee, 2014). To explore both the mechanism of action and the efficacy of Z944 as a potential novel pain therapeutic, we tested the effects of Z944 on putative T-type currents, activity-induced calcium transients and overall membrane excitability in individual lamina I neurons and assessed the analgesic effects of Z944 across doses in a CFA model of inflammatory pain in both male and female adult rats.

2 | METHODS

2.1 | Study approval

These experiments were approved by the institutional Animal Care Committees where experiments were performed (Hospital for Sick Children, University of Toronto, University of British Columbia, Carleton University, and the University of Ottawa Heart Institute; Animal Use Protocol# 111497) and performed in accordance with animal care regulation and policies of the Canadian Council on Animal Care. All animals were housed and cared for in accordance with the recommendations of the Canadian Council for Animal Care.

2.2 | Animals

All experiments were performed on male or female rats supplied by Charles River Laboratories. Sprague Dawley and Wistar rats were selected for this study, as rat spinal tissue provides increased area in comparison with mice, and Sprague Dawley rats have a calm demeanour, making them well-suited for behavioural experiments. Animals for electrophysiological and calcium imaging experiments were completed using male juvenile Wistar rats (P11 to P21, Figure 3 only) or adult (P60–90) Sprague Dawley (SD) rats (325–400 g). All animals were housed in individual high-efficiency particulate air-filtered cages with corn cob bedding, crinkle paper, and a PVC tube for environmental enrichment. Animals were housed with either one or two littermate companions.

Sprague Dawley rats for behavioural experiments were delivered at 3 months of age to account for the weight differences between male and female animals and were housed at the testing facility for a minimum of 5 days before beginning the study. Animal studies are reported in compliance with the ARRIVE guidelines (Percie du Sert et al., 2020) and with the recommendations made by the *British Journal of Pharmacology* (Lilley et al., 2020).

2.3 | Spinal cord isolation

Spinal cords were isolated from juvenile male Wistar rats or adult male SD rats as previously published (Hildebrand et al., 2014, 2011). Briefly, animals were anaesthetized with intraperitoneal injection of 20% (w/v) urethane ($3 \text{ g} \cdot \text{kg}^{-1}$) and killed by severing of the cervical spinal cord and vertebrae. The lumbar region of the spinal cord was dissected from the rat and placed in a protective sucrose dissection solution. Dissection solution contained (mM): 50 sucrose, 92 NaCl, 15 D-glucose, 26 NaHCO₃, 2.5 KCl, 1.25 NaH₂PO₄, 0.5 CaCl₂, 7 MgSO₄, 1 kynurenic acid, bubbled with 5% CO₂/95% O₂ (pH 7.3, 310 mOsm). Dorsal roots and dura were removed from the lumbar cord, and L4–L6 were removed from the rest of the cord. The L4–L6 piece was then glued against an agar block (4% agarose in distilled water) and placed in a Leica VT 1000s or 1200s vibratome (Leica, Germany) containing ice-cold sucrose dissection solution. Parasagittal slices (300 μm thick) were obtained from the vibratome. Slices were then incubated in dissection solution lacking **kynurenic acid** at 34°C for 40 min and then cooled passively to room temperature (21 to 22°C for ≥ 30 min) before electrophysiological recording and calcium imaging.

2.4 | Electrophysiology of spinal cord lamina I neurons

For data in Figure 1, slices were placed under an upright Olympus BX51WI microscope (Olympus Corporation, USA) with a 40 \times water immersion objective. Lamina I neurons were identified based on location relative to myelin tracts and substantia gelatinosa, and patched into with recording pipettes of 6–8 M Ω , pulled by a Sutter P97 puller (Sutter Instruments, USA). The internal voltage-clamp patch pipette solution consisted of (mM) 105 D-gluconic acid, 105 CsOH, 17.5 CsCl, 10 EGTA, 10 HEPES, 2 Mg-ATP, 0.5 Na₂-ATP (pH 7.3, 290 mOsm). The external recording solution (artificial CSF) consisted of (mM) 125 NaCl, 20 D-glucose, 26 NaHCO₃, 3 KCl, 1.25 NaH₂PO₄, 2 CaCl₂, 1 MgCl₂, and 0.04 Alexa Fluor-488 or -594 (pH 7.3, 310 mOsm). Perfusion speed was 1 ml \cdot min⁻¹, and the solution was continually bubbled with 5% CO₂/95% O₂. The recording solution also contained 0.5 μM **tetrodotoxin** and 5 mM **tetraethylammonium** to block voltage-gated sodium channels and voltage-gated potassium channels, respectively. All recordings were performed at room temperature. Morphology of lamina I neurons was determined after recording by using the fine focus to move through the z-plane and identify the number of primary dendrites. Neurons with two primary dendrites were classified as fusiform and similarly, neurons with three or four primary dendrites were classified as pyramidal or multipolar, respectively (Figure S1) (Lima & Coimbra, 1986).

Patch-clamp recordings were made using a Multiclamp 700B amplifier (Molecular Devices, CA, USA) and a Digidata 1550B Digitizer (Molecular Devices, CA, USA) connected to a desktop computer with pClamp 10.7 software. Voltage-clamp recordings were digitized at 10 KHz and low-pass filtered at 2 KHz. Recordings were

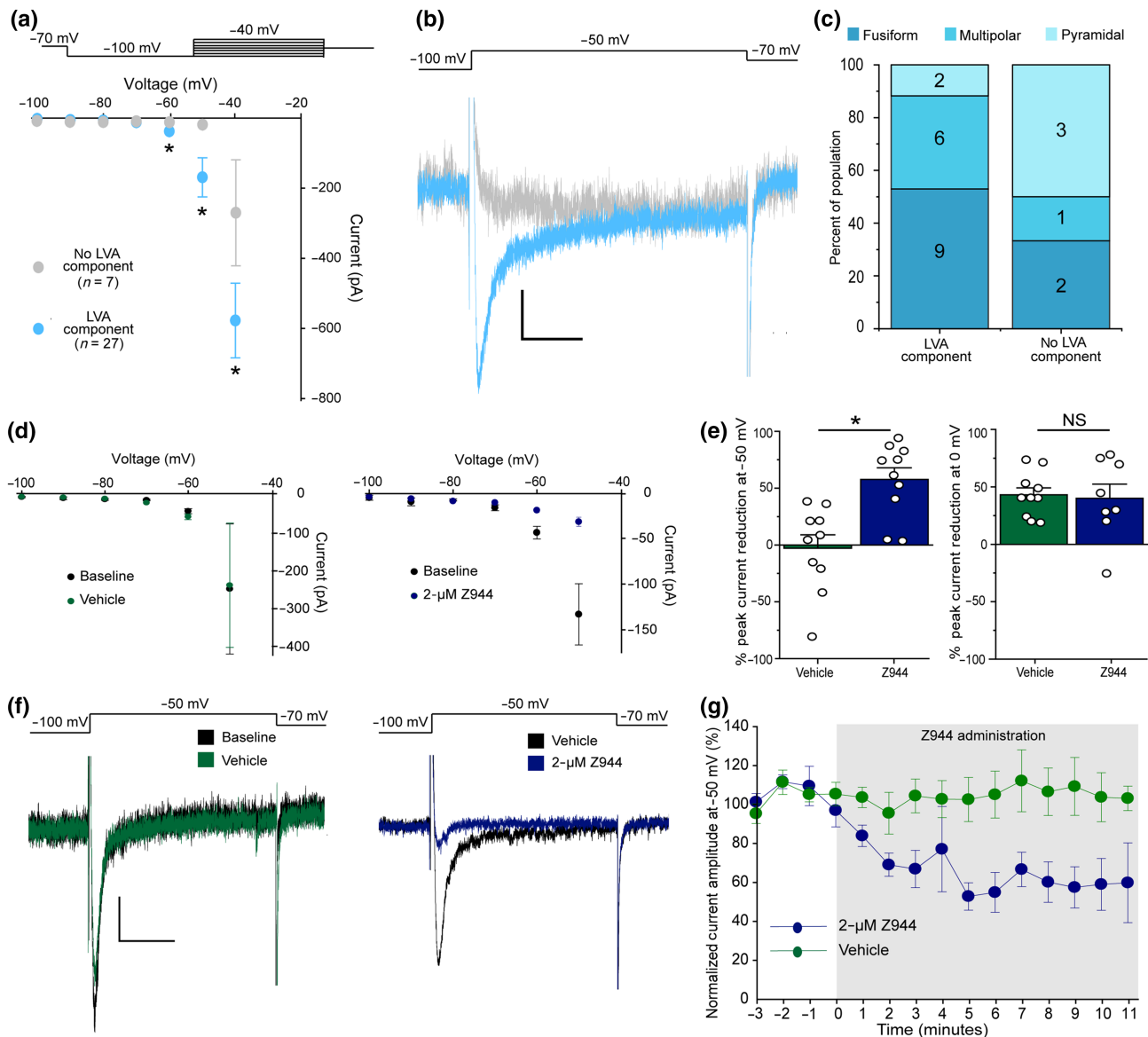


FIGURE 1 Z944 selectively reduces inward current through low voltage-activated calcium channels in spinal cord lamina I neurons. (a) Top: Voltage-clamp protocol used to measure calcium currents in lamina I neurons. Neurons were hyperpolarized to -100 mV for 500 ms, before a 500-ms step current injection beginning at -100 mV and increasing by 10 pA each sweep. Bottom: Analysis of calcium currents revealed two populations of lamina I neurons; those with a low voltage-activated (LVA) component (27/34, light blue), and those lacking an LVA component (7/34, light grey circles). Peak current with steps to -60 , -50 and -40 mV was compared between neurons with and without an LVA component using unpaired Mann-Whitney t -tests (-60 mV: $P < .05$, -50 mV: $P < .05$, -40 mV: $P = .05$). (b) Current traces in example neurons with an LVA component (light blue) and without an LVA component (light grey) for a voltage step from -100 mV to -50 mV. Scale bar y axis = 20 pA, x axis = 100 ms. (c) Distribution of morphologies in a subset of recorded neurons. Where possible, neurons were classified into three main morphologies. (d) In a subset of neurons with an LVA component, IV-curves were plotted for baseline recordings and after vehicle ($n = 8$ neurons, left, green) or Z944 ($n = 10$ neurons, 2 μ M, right, blue) administration. (e) Left: Quantification of percent peak current reduction at -50 mV for vehicle (green) and Z944 (blue) administration (Student's unpaired t -test, $P < .05$, $n = 10$ neurons for both conditions). Right: Quantification of percent peak current reduction at 0 mV for vehicle (green) and Z944 (blue) administration (Student's unpaired t -test, $n = 10$ neurons for vehicle and 8 neurons for Z944). (f) Sample current traces induced by depolarization from -100 mV to -50 mV. Left: Before (black) and after vehicle (green) administration. Right: Before (black) and after Z944 administration. Scale bar y axis = 20 pA, x axis = 150 ms. (g) Time course of peak current at -50 mV, normalized to first 3 min before administration of either vehicle (green, $n = 6$ neurons), or Z944 (blue, $n = 6$ neurons). All error bars represent \pm SEM. * $P < .05$

included for analysis only if they maintained a leak current more positive than -50 pA at -60 mV and if access resistance began below 25 M Ω and did not change by more than 30% during the

recording period. The IV-curve protocol started at -60 mV, with a 500-ms step hyperpolarization to -100 mV, followed immediately by incremental steps from -100 mV, increasing by 10 mV (up to

–40 mV). For time course experiments, steps began from –70 mV and were repeated continuously at a rate of once per min. For these experiments, drug wash-in experiments were randomized such that Z944 and DMSO vehicle trials were completed in alternating order where possible. Blinded analysis was not possible given that only the experimenter had the expertise required for this specific analysis. Statistical analysis in Figure 1a,e was performed on groups of unequal size, due to differing population sizes from an unbiased sampling of all neurons in lamina I and due to exclusion of two neurons from analysis in the DMSO vehicle group due to significant changes in input resistance, respectively. Statistical analysis was not performed on the data in Figure 1c due to group sizes of $n < 5$ but was included as evidence that all morphological classes can either possess or lack a T-type component.

For data within Figure 3, slices were placed under an Axioskop 2 FS plus microscope under infrared-differential interference contrast optics (Zeiss, Germany). All other parameters were the same as Figure 1, except the internal current-clamp patch pipette solution consisted of (mM) 140 K-gluconate, 4 NaCl, 0.5 MgCl₂, 10 HEPES, 4 Mg-ATP, 0.5 Na₂-ATP, 1 EGTA (pH 7.3, 290 mOsm). The junction potential for current-clamp was calculated as 14.6 mV (i.e., –50 mV = –64.6 mV) (Junction potential calculator, Clampex) and has been corrected in all experimental data. Recordings were included for analysis only if they maintained a resting membrane potential below –50 mV and if first action potentials reached a minimum of +5 mV. Bridge balance and pipette capacitance compensation were performed in all neurons and corrected prior to each recording. In all experiments, neurons were held between –60 and –70 mV (typically 0 to –20 pA holding current injection). VI-curves were run from a holding potential of –60 to –70 mV, and incremental step current injections were performed from –40 pA, with 10 pA steps (1200 ms duration). Drug wash-in experiments were randomized such that Z944 and DMSO vehicle trials were completed in alternating order where possible. Statistical analysis in Figure 3e was performed on groups of unequal size, due to variability in the number of neurons that met the criteria for recordings and analysis. Statistical analysis was not performed on Figure 3b due to group sizes of $n < 5$ but was included as a representative expansion of data presented in Figure 3c.

For pharmacology experiments, Z944 was first dissolved in DMSO and then added to the external recording solution, such that final DMSO concentration was always below 0.1%. Washout experiments are problematic in spinal slice recording assays, with the potential for hydrophobic compounds to stick to myelin and cell membranes as well as to change excitability measures over the longer time durations required for washout. Moreover, we have previously found that the Z944-mediated inhibition of T-type currents in reticular nucleus neurons of thalamic slices was largely non-reversible after 30 min of washout (Tringham et al., 2012). Here, we therefore tested for net effects of Z944 in superficial dorsal horn neuron recordings by comparing with cells that were treated with vehicle for the same durations and under the same experimental conditions. For vehicle experiments, DMSO without Z944 was added. For all electrophysiology experiments, perfusion of Z944 or vehicle was 10–15 min.

2.5 | Simultaneous electrophysiology and two-photon calcium imaging of lamina I neurons

Spinal cord lamina I neurons were recorded from in current-clamp configuration, with simultaneous two-photon calcium imaging as previously described (Harding et al., 2020). Briefly, slices were placed under a Zeiss 710 NLO system equipped with an AxioExaminer Z1 (Zeiss, Germany), and neurons were visualized under infrared-differential interference contrast optics. Patch-clamp recordings were made with recording pipettes of 7–10 M Ω , pulled by a Sutter P97 puller (Sutter Instruments, Navato, CA, USA). The external recording solution (artificial CSF) and perfusion speed was as above. The internal current-clamp patch pipette solution consisted of (mM) 112 K-gluconate, 8 KCl, 10 HEPES, 4 Mg-ATP, 0.3 Na₂-ATP, 10 phosphocreatine, 0.3 EGTA, 0.04 Alexa Fluor-594, 0.11 Oregon Green Bapta-1 (pH 7.3, 290 mOsm). Neurons were allowed to dialyze for 20–30 min before imaging to allow the fluorescent dye concentration to equilibrate. All recordings were performed between 24°C and 28°C. Current-clamp recordings were performed as above. Bridge balance and pipette capacitance compensation were performed in all neurons. In all experiments, neurons were held between –70 and –80 mV (typically 0 to –20 pA holding current injection). Single action potentials were evoked with a 5 ms current injection of between 150 and 400 pA. Each recording was 15 s in duration, with the experimental current injection at 2 s into recording. A minimum of 15 s was given between the end of one recording and the beginning of the next to allow the neuron to return to baseline.

Two-photon dual excitation of OGB-1 (110 μ M in recording pipette) and AF-594 (40 μ M in recording pipette) was achieved using a Coherent Chameleon Ultra Ti:Sapphire laser tuned to 800 nm (Coherent, USA). OGB-1 and AF-594 fluorescence were split based on emission spectra using NDD filter cubes (500–550 nm, 565–610 nm; Carl Zeiss Microscopy, Germany) and sent into NDD detectors (Carl Zeiss Microscopy, Germany). Two-photon images were obtained using a 20 \times water-immersion objective lens (Carl Zeiss Microscopy, Germany) and the Zen 2009 acquisition program (Carl Zeiss Microscopy, Germany). Laser power was kept between 0.3% and 0.7%, and gain was restrained to 650–850 for all calcium imaging experiments. Fluorescence data were acquired using line scan acquisition (1024 pixels \times 1 pixel line scan, 2 \times averaging) at a rate of 133 Hz and saved as LSM files from Zen 2009 (Carl Zeiss Microscopy, Germany). Calcium imaging data were analysed as previously described, utilizing a custom-made, semi-automated MATLAB toolbox (Mathworks, USA) for analysis, entitled CIAT (Calcium Imaging Analysis Toolbox) (Harding et al., 2020). Use of the semi-automated analysis toolbox, Calcium Imaging Analysis Toolbox, which automatically calculates peak response from averaged calcium imaging trials, was designed to remove experimental bias. For data in Figure 2, drug wash-in experiments were randomized such that Z944 and DMSO vehicle trials were completed in alternating order where possible. Statistical analysis within this figure was performed on groups with an $n > 5$, of unequal size due to one neuron being removed for photobleaching.

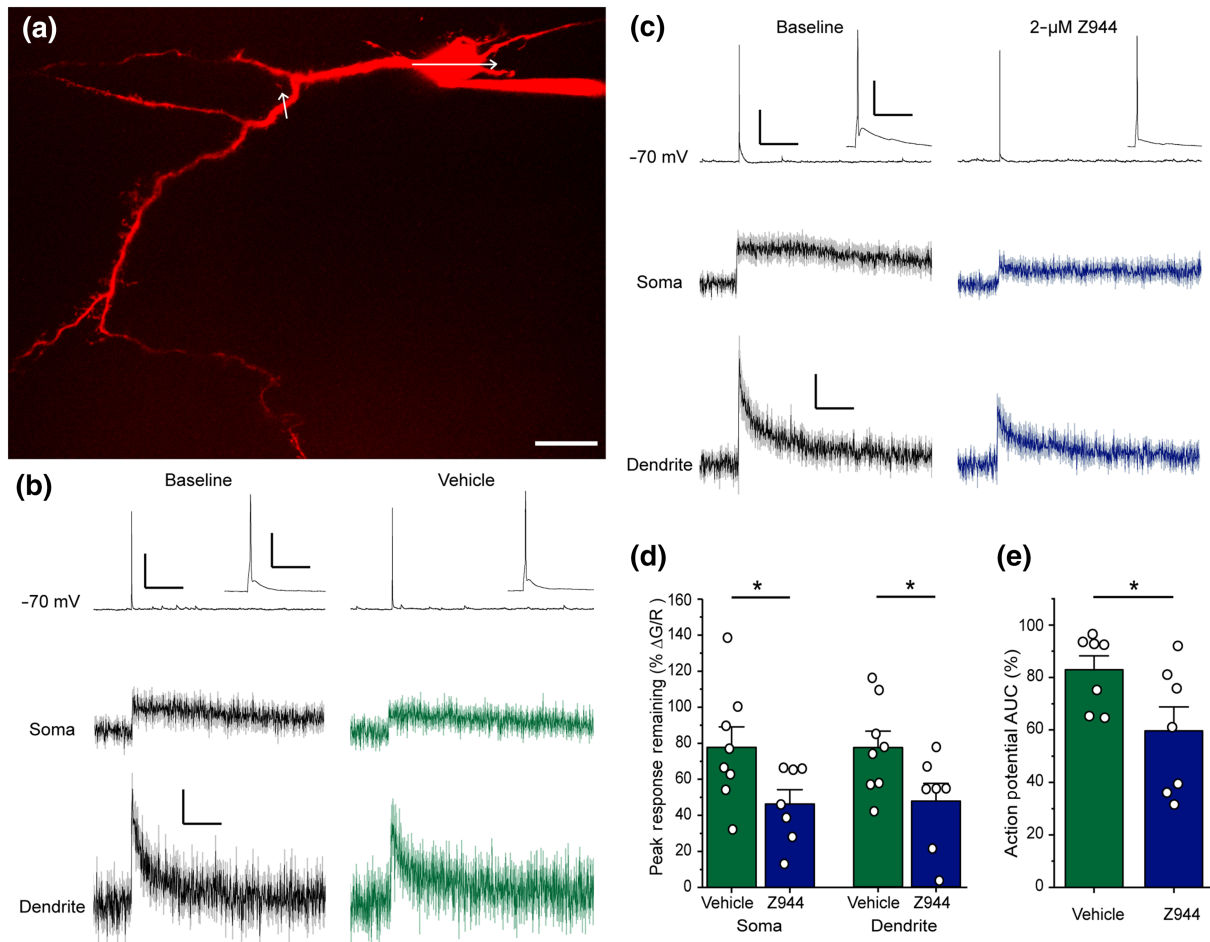


FIGURE 2 Activity-induced calcium transients in lamina I neurons are reduced by Z944. (a) Flattened projection of a two-photon z-stack of a lamina I neuron filled with Alexa Fluor-594 via a patch pipette. White arrows represent line scan trajectory during calcium imaging. Scale bar represents 20 μm . (b) Left: Single action potentials induced by current injection (5 ms, 200 pA) from a membrane potential of -70 mV induce calcium transients in the somata and dendrites of lamina I neurons (black). Right: Recordings remain stable after vehicle administration (green, right). Traces are an average of eight neurons for both somatic and dendritic compartments. (c) Wash-in of Z944 (2 μM) greatly reduces calcium transients in both the somata and dendrites (dark blue) and decreases action potential afterdepolarization (insets). Traces are an average of seven neurons for both somatic and dendritic compartments. For b and c, action potential traces are representative examples from a single neuron, calcium transients are average responses, \pm SEM. For b and c, electrophysiology scale bar y axis = 30 mV, x axis = 2 s. Inset scale bar y axis = 30 mV, x axis = 100 ms. Calcium imaging scale bar y axis = $\Delta\text{G/R}$ 0.04, x axis = 2 s. (d) Quantification of the percent remaining peak calcium transient, as displayed in b and c after the administration of Z944 or vehicle. Comparisons performed with Student's unpaired t-tests ($P = .05$ for soma, $P < .05$ for dendrite, $n = 8$ neurons for vehicle and 7 neurons for Z944 for both compartments). (e) Quantification of the percent remaining action potential area under the curve after administration of Z944 or vehicle ($P = .05$, Student's unpaired t-test, $n = 7$ neurons for Z944 and vehicle conditions). * $P < .05$ for all t-tests. All error bars represent SEM

2.6 | Freund's adjuvant model of inflammatory pain and behaviour testing

Animals were housed in pairs, had free access to food and water, and were randomly assigned to their respective experimental groups. Group sizes for behavioural experiments (Figure 4) were set to 10 animals per group based on previous study design (Dedek et al., 2019) and a priori sample size calculation for repeated measures ANOVA for within-group differences using G*Power 3.1.9.7 (Heinrich-Heine-Universität Düsseldorf) based on the following parameters: a moderate effect size of 0.20, $\alpha = 0.05$, power = 0.99, number of groups = 4 (Figure 4a,c) and 5 (Figure 4e),

13 measurements, correlation among repeated measures = 0.5, and nonsphericity correction $\epsilon = 1$. These parameters yielded a total sample size of 36 for Figure 4a,c and 35 for Figure 4e. Total sample size was rounded up to 10 animals per group to ensure equal group samples and to ensure adequate power if an animal needed to be removed from the study. Two animals were withdrawn from the study and killed early because they injured each other in a fight. Animal husbandry was performed exclusively by the tester for the entire duration of the animals' stay at the housing facility. Cohorts of male and female animals were run separately; however, in some instances, male and female animals were housed in the same room concurrently. In cases when the housing room had both male and female rats, husbandry for female

animals was performed before any male cages were opened. Cohorts were run in groups of eight to 10 animals. Lab coats and gloves were changed between cohorts. The housing room was used exclusively for this study and was open to only the experimenter (female) and animal care staff (who did not open cages or handle the animals).

Complete Freund's adjuvant (CFA, Sigma) was used to model inflammatory pain. Rats were given a 0.3-ml plantar injection of either phosphate-buffered saline (PBS: saline) or CFA (a 50% by volume mixture of CFA and PBS) under isoflurane anaesthesia. Blinding was not performed for CFA injections, as the tester also performed injections and all animal husbandry, and the effects of CFA injection are obvious while handling the animals and performing testing. Animals were left to acclimate to their behaviour testing chambers for 45 min before testing each morning. Tests were performed at approximately the same time each day, across cohorts, for the duration of the study. Behaviour testing for pain hypersensitivity was performed using von Frey filaments to measure mechanical paw withdrawal threshold. Withdrawal threshold was measured in the injected paw using the simplified up-down method, as described by Bonin et al. (2014). Measurements were taken at baseline (pre-injection) and then at 24, 48 and 72 h post-CFA or PBS injection. We report paw withdrawal threshold in grams, as labelled on each von Frey filament. As per simplified up-down method, an adjustment factor is used to determine the paw withdrawal threshold for each trial. We used an adjustment factor of ± 0.5 (difference, in grams, between filaments).

2.7 | Intraperitoneal injection (i.p.)

Seventy-two hours following subplantar injection of CFA and following Day 3 behaviour testing (see above), male and female adult Sprague-Dawley rats were given an i.p. injection of 1, 3 or 10 mg.kg⁻¹ Z944 or vehicle dissolved in 0.5% (weight/volume) of carboxymethylcellulose (Sigma Aldrich, USA). Z944 is highly bioavailable and CNS-penetrant, with pharmacokinetic studies demonstrating that oral and systemic administration produces low micromolar concentrations of Z944 in rodent plasma (unpublished observations and Casillas-Espinosa et al., 2019). Moreover, i.p. injection of 10 mg.kg⁻¹ Z944 reduced brain epileptiform activity in adult rats (Tringham et al., 2012), demonstrating CNS penetrance and actions on central excitability at the dose and route of administration of Z944 used here. Z944 was dissolved in DMSO to create a stock solution (100 mg.ml⁻¹ for animals receiving 10 mg.kg⁻¹, 30 mg.ml⁻¹ for animals receiving 3 mg.kg⁻¹, and 10 mg.ml⁻¹ for animals receiving 1 mg.kg⁻¹) that was then suspended in the carboxymethylcellulose solution (1-part Z944 stock: 9-part carboxymethylcellulose solution). Vehicle-treated animals received DMSO without Z944 in 0.5% (weight/volume) of carboxymethylcellulose solution. All solutions were prepared the day of injection, and the experimenter was blinded to the treatment by a lab-mate. All animals were allowed 20 min in their home cage between Day 3 testing and the administration of the i.p. injection. This allowed animals to eat or drink before being placed back in testing chambers for the time course. Animals received injections 1–1.5 min

apart, with the exact time noted by the experimenter to ensure accurate readings during the time course. Intraperitoneal injection was performed by the experimenter alone using a surgical drape to restrain the animal. After i.p. injection, animals were placed in the behaviour testing chambers and allowed to acclimate for 20 min. During the time course, measurements of paw withdrawal threshold were taken every 15 min, starting 20 min after i.p. injection. The time of the test was measured from the third stimulus administration (five stimuli were presented in each trial, and the third, the middle stimulus, occurred at the given time interval). We found that i.p. injection of Z944 (1 to 10 mg.kg⁻¹) did not induce any behavioural signs of sedation or motor deficits. Moreover, a previous in-depth analysis of potential non-specific *in vivo* effects of Z944 demonstrated that i.p. injection of Z944 at a dose above that used in the present study (30 mg.kg⁻¹) did not induce any significant sedation or motor abnormalities (Tringham et al., 2012).

The technique for measuring paw withdrawal threshold differed during the time course. Simplified up-down method normally involves two trials of five stimuli that are then averaged to give paw withdrawal threshold. For the time course, only one trial was performed every 15 min to ensure that the animals were not over-stimulated. A pilot study was used to determine an effective interval for the time course. One unsuccessful pilot was run using a testing interval of 10 min. This pilot was deemed unsuccessful because animals were displaying freezing behaviour: not reflexively withdrawing their paw at weights normally far-above expected withdrawal threshold. We concluded that allowing animals more time to recover between trials was necessary and thus increased the testing interval by 50%. This decision, in turn, allowed more accurate timing of testing at each animal's given testing time. Animals were sacrificed immediately after the conclusion of the time course.

2.8 | Materials

Unless otherwise indicated, all compounds were obtained from Sigma Aldrich (USA). Z944 (N-[[1-[2-(tert-butylamino)-2-oxoethyl]piperidin-4-yl]methyl]-3-chloro-5-fluorobenzamid) was synthesized as previously described (Tringham et al., 2012).

2.9 | Data and analysis

This manuscript complies with BJP's recommendations and requirements on experimental design and analysis (Curtis et al., 2018). Data in some figures of this manuscript have been normalized to reduce variability. In Figure 1e, data are plotted as % peak current reduction within each neuron (post/pre) to allow direct comparison of Z944 effects as compared with a DMSO control. In Figure 1g, data are plotted as normalized % current, representing the percent change in average current for each neuron within the first 3 min of recording (post/pre). In Figure 2d,e, data are plotted as % peak calcium transient remaining and % AUC remaining (post/pre) to account for rundown

effects in the DMSO control, allowing for better comparison of the true effect of Z944. For all experiments in all figures, no analysis was performed to determine presence of outliers, and therefore, all data points were included for analysis.

For all statistical analysis, $P < .05$ was used as the threshold for statistical significance, and in all experiments, the declared group size is the number of independent values, and statistical analysis was performed upon these values. Statistical analysis was only performed when group size was at least $n = 5$, which reflects the number of independent, non-technical replicate values. Sample sizes for experiments in Figures 1–3 were determined based off of previous studies (Harding et al., 2020; Hildebrand et al., 2014), and data in these figures were analysed with Sigmaplot 12.0 (Systat Software, USA). Prior to running Student's paired t -tests, the normality of the data was tested (Shapiro–Wilk test) and if the data failed this test of normality ($P < .05$), a Wilcoxon signed-rank test was performed in lieu of a Student's paired t -test. t -tests comparing the means from different

neurons or animals were performed as unpaired t -tests. If the data failed a test of normality (Shapiro–Wilk test), then a Mann–Whitney rank sum test was performed instead. All two-way ANOVA post hoc comparisons were performed using the Holm–Sidak method. The post hoc tests were conducted only if F in ANOVA achieved statistical significance ($P < .05$) and showed no significant variance in homogeneity. Statistical analysis involved sample sizes of at least 5 per group ($n = 5$), where $n =$ number of independent values.

Within Figure 4, comparisons of means were performed using unpaired Mann–Whitney t -tests, due to failure of Shapiro–Wilk normality test (Sigmaplot 12.0, Systat Software, USA). One-way repeated-measures ANOVAs were performed using SPSS (IBM SPSS Statistics 25.0, see Tables S1 and S3). Before running each ANOVA, we examined Mauchly's test of sphericity, which indicated that the assumption of sphericity was violated in each case (see Tables S1 and S3). In each case, the Greenhouse–Geisser epsilon adjustment of degrees of freedom was deemed the most appropriate adjustment,

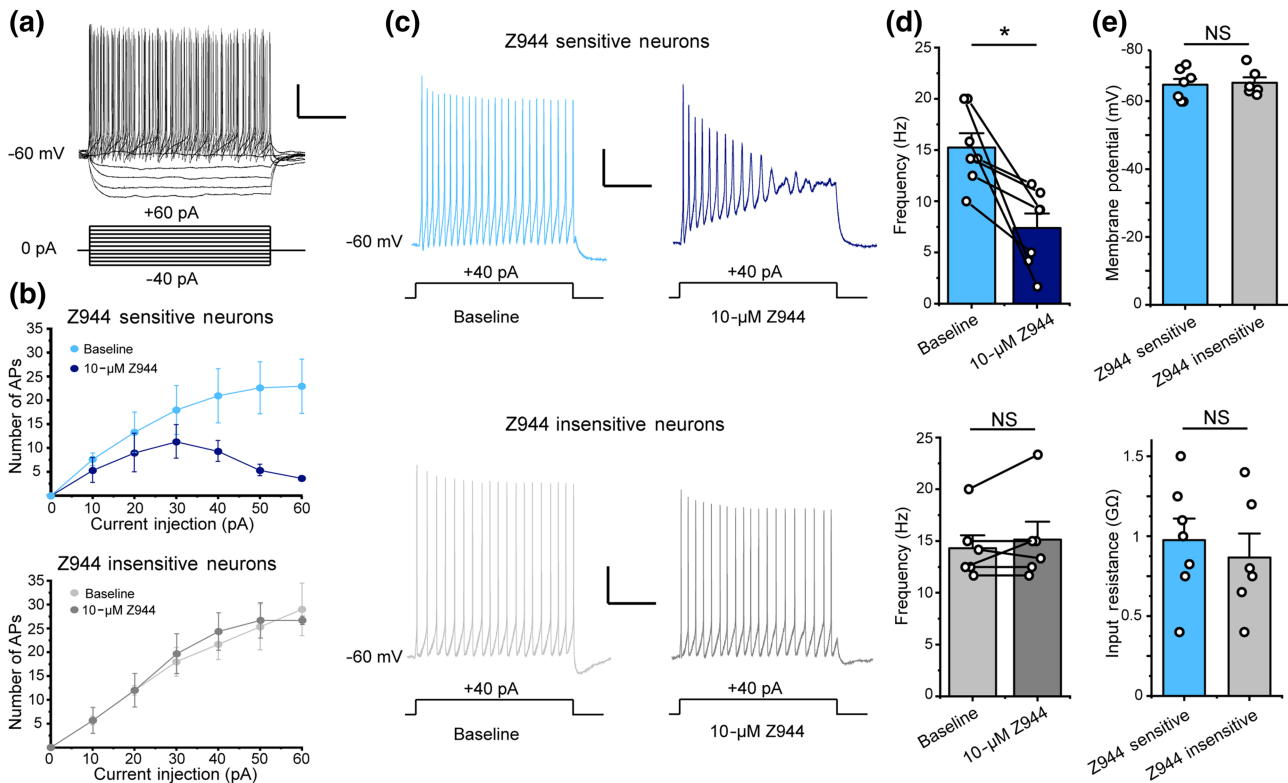


FIGURE 3 Z944 reduces excitability in a subset of laminae I/II spinal cord neurons. (a) Representative membrane potential trace of a lamina I/II neuron in response to step current injection (1200 ms) beginning from -40 pA and increasing by 10 pA each step. (b) Top: Administration of Z944 ($10 \mu\text{M}$) inhibited action potential firing in a subset of laminae I/II neurons, while having no effect on action potential firing for the remaining laminae I/II neurons (bottom). Action potentials were counted during each step current injection in a subset of neurons, revealing a population of neurons with reduced firing after the administration of Z944 (baseline = light blue, Z944 = dark blue; $n = 3$ neurons) and a population insensitive to Z944 administration (baseline = light grey, Z944 = dark grey; $n = 3$ neurons). (c, d) The effects of Z944 on excitability were evaluated for depolarizing current injection steps that elicited 10- to 20-Hz AP firing for each individual laminae I/II neuron (typically ~ 40 pA). Administration of Z944 ($10 \mu\text{M}$) significantly inhibited action potential firing in a subset of laminae I/II neurons (top, 7/13 neurons) ($P < .05$, Student's paired t -test), while having no effect on action potential firing for the remaining laminae I/II neurons (bottom, 6/13 neurons) ($P > .058$, Student's paired t -test). For a and c, electrophysiology scale bar y axis = 20 mV, x axis = 400 ms. (e) The input resistance and resting membrane potential of Z944-sensitive laminae I/II neurons were not significantly different than Z944-insensitive neurons ($P > .05$, Student's unpaired t -tests, $n = 7$ neurons for Z944-sensitive group and 6 neurons for Z944-insensitive group). All error bars represent mean \pm SEM. * $P < .05$

since in each case, it was below 0.75 (Tables S1 and S3) and was thus used to determine the *P* value. Bonferroni's significant difference test followed ANOVAs when *F* in ANOVA achieved statistical significance ($P < .05$) and showed no significant variance in homogeneity (Tables S2 and S4). * $P < .05$ for all figures.

2.10 | Nomenclature of targets and ligands

Key protein targets and ligands in this article are hyperlinked to corresponding entries in the IUPHAR/BPS Guide to PHARMACOLOGY <http://www.guidetopharmacology.org> and are permanently archived in the Concise Guide to PHARMACOLOGY 2019/20 (Alexander et al., 2019).

3 | RESULTS

3.1 | Z944 reduces inward current through low voltage-activated calcium channels in a subset of lamina I neurons

To determine if T-type channels are present in lamina I spinal dorsal horn neurons, we first recorded calcium channel currents from visually identified lamina I neurons within parasagittal spinal cord slices of adult male rats. The voltage threshold for activation of calcium currents was identified for each recorded neuron by analysing IV-curves. Of 34 recorded neurons, 27 exhibited a rapidly inactivating inward current beginning at -60 mV, consistent with the presence of low voltage-activated T-type calcium channels (Figure 1a,b) (Weiss & Zamponi, 2019). In seven of 34 neurons, only a slower inactivating inward current was detected at depolarizations beginning at -40 mV, consistent with the biophysical properties of high voltage-activated calcium channels. As such, we defined this neuronal subpopulation as one with no measurable low voltage-activated T-type component.

Distinct subpopulations of lamina I neurons can be delineated by morphology (Lima & Coimbra, 1986). We therefore classified the morphology of Alexa Fluor-filled neurons after recording (Figure S1) and compared the distribution of morphologies for lamina I neurons that did and did not contain the low voltage-activated T-type component. Of the neurons with a low voltage-activated component where morphology could be definitively determined, 9/17 were fusiform, 6/17 were multipolar, and 2/17 were pyramidal (Figure 1c). Of those without a low voltage-activated component, 2/6 were fusiform, 1/6 was multipolar, and 3/6 were pyramidal. Although there was a bias towards fusiform neurons containing a low voltage-activated component, and pyramidal neurons not containing a low voltage-activated component, group sizes were too small to perform statistical analysis (Figure 1c). However, from these exploratory results, we can conclude that low voltage-activated currents are found in a large subset of lamina I neurons and are not restricted to specific morphological subtypes.

We next sought to determine whether Z944 application affects the low voltage-activated component of calcium currents present in $\sim 80\%$ of lamina I neurons. While perfusion of artificial CSF with DMSO vehicle did not affect low voltage-activated currents at -60 and -50 mV, administering $2 \mu\text{M}$ Z944 reduced these low voltage-activated currents at both potentials (Figure 1d,e). In a subset of neurons, we analysed the time course of low voltage-activated current block by Z944 using repeated test pulses to -50 mV (Figure 1f, g). We found that within the first minute of Z944 administration, peak current dropped by 20% and reached a plateau inhibition of 40–50% within 5 min. Overall, Z944 treatment resulted in a significant reduction in calcium currents elicited at -50 mV as compared with DMSO control-treated neurons ($n = 10$ neurons for both conditions). No significant effect of Z944 compared with control treatment was observed for high voltage-activated calcium currents elicited at 0 mV ($n = 10$ neurons for vehicle and 8 neurons for Z944) (Figure 1e), indicating specificity to T-type channels. Altogether, the presence of rapidly inactivating low voltage-activated calcium currents and their selective inhibition by Z944 strongly supports the conclusion that T-type currents are present in $\sim 80\%$ of lamina I neurons of adult rats, encompassing all three main morphologically-defined neuron subpopulations.

3.2 | Activity-induced calcium transients in spinal cord lamina I neurons are reduced by Z944

Activity-dependent intracellular calcium signalling in lamina I neurons has been demonstrated to lead to hyperexcitability and pathological pain (Ikeda et al., 2003; Wei et al., 2006). We have recently shown that single action potentials drive increases in intracellular calcium concentration at both the soma and dendrites of lamina I neurons, through a mechanism dependent upon voltage-gated calcium channels (Harding et al., 2020). Given our identification here of T-type currents in the majority of lamina I neurons, we next used a combination of current-clamp recordings and simultaneous two-photon calcium imaging to test whether Z944 can attenuate activity-induced calcium responses in these critical nociceptive spinal neurons.

Lamina I neurons were filled with the calcium-sensitive fluorophore Oregon Green Bapta-1, and the structural fluorophore Alexa Fluor-594 via the patch pipette and single action potential-induced calcium responses were measured in the soma and primary dendrites, as previously described (Figure 2a) (Harding et al., 2020). We found that, on average, perfusion of $2 \mu\text{M}$ Z944 significantly decreased action potential-induced calcium responses in both the soma and dendrites, as compared with the DMSO vehicle control ($n = 8$ neurons for vehicle and 7 neurons for Z944; Figure 2b–d). Interestingly, we also found that perfusion of Z944 significantly decreased the area under the curve for action potential waveforms, as compared with the DMSO vehicle control ($n = 7$ neurons for Z944 and vehicle conditions; Figure 2d). This decrease in area under the curve corresponded to a visible reduction in the action potential afterdepolarization

following Z944 treatment (Figure 2c). Our findings that Z944 significantly reduced action potential-evoked calcium responses by over 50% in both the soma and dendrites of lamina I neurons indicates that T-type calcium channels are the predominant mediators of this action potential-evoked calcium signal.

3.3 | Z944 reduces excitability in a subset of superficial dorsal horn spinal cord neurons

Given our findings that Z944 decreases activity-induced calcium responses and reduces action potential afterdepolarizations, we next sought to determine whether administration of Z944 affects the overall excitability of superficial dorsal horn nociceptive neurons. We therefore tested the effects of Z944 on trains of action potentials in a combined population of laminae I and II superficial dorsal horn neurons, with stepwise test current injections increasing by +10 pA increments and the number of evoked action potentials calculated for each depolarizing current step (Figure 3a,b). For each neuron, we identified a depolarizing test current injection step (+10 to +50 pA) that evoked action potential firing in the 10- to 20-Hz frequency range, which corresponds to physiological firing rates induced by nociceptive input (Keller et al., 2007) (Figure 3c). Administration of vehicle DMSO control for 10 to 15 min did not significantly alter the frequency of action potential firing at these test current injection steps (baseline 15.5 ± 1.6 Hz, DMSO 17.0 ± 2.0 Hz, $n = 5$ neurons, data not shown).

We next administered Z944 for 10 to 15 min at a concentration (10 μ M) that completely abolishes T-type currents in thalamic slices (Tringham et al., 2012) and measured the effects of Z944 on 10 to 20 Hz action potential firing (Tringham et al., 2012). We found that superficial dorsal horn neurons could be separated into those that responded to 10 μ M Z944 with a significant decrease in action potential firing frequency ($48.7 \pm 10.6\%$ reduction, 7/13 neurons) and those that showed no response to this elevated concentration of Z944 ($-5.1 \pm 4.3\%$ reduction, 6/13 neurons) (Figure 3c,d). In a subset of recorded neurons, we investigated the full relationship between current injected and number of action potentials evoked and found that the Z944-mediated decrease in action potential number for Z944-sensitive neurons (3 of 6 neurons) was observed at all current injection amplitudes but was most pronounced with larger current injections of +50 and +60 pA (Figure 3b). Importantly, the differential effects of Z944 between superficial dorsal horn neuron subpopulations were not due to differences in passive membrane properties, as both resting membrane potential and input resistance were not significantly different between Z944-sensitive and Z944-insensitive neurons (Figure 3e). Our finding that administration of Z944 significantly reduces the firing frequency of over half of superficial dorsal horn neurons strongly suggests that postsynaptic T-type channels shape the excitability of these nociceptive spinal neurons and could therefore be an important target for reducing nociceptive input that ascends to the brain.

3.4 | Intraperitoneal injection (i.p.) of Z944 reverses CFA-mediated tactile allodynia in a dose-dependent manner

Having demonstrated that Z944 decreases superficial dorsal horn neuron excitability through inhibition of postsynaptic T-type channels, we next sought to determine whether Z944 can produce analgesia in a rodent complete Freund's adjuvant (CFA) model of inflammatory pain. The CFA model of inflammatory pain includes a spinal sensitization component that mediates prolonged pain hypersensitivity (Ren et al., 1992). Intraplantar injection of CFA induced a robust decrease in mechanical paw withdrawal threshold compared with baseline measures (Day 0), corresponding to tactile allodynia, which was not observed in saline control-injected rats (Figure 4a). Three days after CFA injection, Z944 or a DMSO vehicle control were i.p.-injected, and paw withdrawal threshold was measured every 15 min for 140 min post injection. The initial tested dose of Z944 (10 $\text{mg}\cdot\text{kg}^{-1}$) has previously been shown to cross the blood brain barrier and attenuate absence seizure activity in the brain (Tringham et al., 2012). We found that i.p. injection of Z944 significantly reversed the CFA-mediated decrease in paw withdrawal threshold compared with vehicle injections from 50 to 125 min post-injection (Figure 4a). In males, i.p. injection of Z944 (10 $\text{mg}\cdot\text{kg}^{-1}$) resulted in $86 \pm 12\%$ anti-allodynia, while injection of a DMSO vehicle produced $3 \pm 1\%$ anti-allodynia ($n = 10$ animals for Z944 and 9 animals for DMSO, Figure 4b), as measured at the peak effect (80 min post i.p. injection).

A major barrier to translation of potential pain therapeutics for use in humans is that the majority of preclinical investigations have typically been performed exclusively in male rodents (Mogil, 2012). As spinal mechanisms of chronic pain differ between males and females (Sorge et al., 2015) and the effects of T-type antagonists on pain sensitivity have not been compared between sexes, we next tested if inhibition of T-type channels with Z944 would reverse mechanical allodynia in CFA-injected female rats. In females, i.p. injection of 10 $\text{mg}\cdot\text{kg}^{-1}$ Z944 resulted in $105 \pm 15\%$ anti-allodynia, while injection of a DMSO vehicle produced $6 \pm 3\%$ anti-allodynia ($n = 10$ animals, Figure 4c,d). Both the time course and magnitude of anti-allodynia produced by Z944 was similar between male and female CFA-injected rats (Figure 4a-d). Importantly, i.p. injection of Z944 had no effect on paw withdrawal threshold in control male ($n = 10$ animals, Figure 4a) and female ($n = 10$ animals, Figure 4c) rats injected with intraplantar saline. This demonstrates that Z944 did not alter baseline mechanical sensitivity and thus did not alter withdrawal responses through non-specific locomotor or sedative effects, but rather selectively reversed CFA-mediated mechanical allodynia in both sexes.

Finally, we sought to determine whether lower doses of i.p.-injected Z944 (1 $\text{mg}\cdot\text{kg}^{-1}$, 3 $\text{mg}\cdot\text{kg}^{-1}$) would reverse mechanical allodynia and whether Z944 exhibits a sigmoidal dose-dependent analgesic relationship typical of many clinically available analgesics (Kuo et al., 2015). Overall, we found that all doses (1, 3 and 10 $\text{mg}\cdot\text{kg}^{-1}$) of Z944 produced anti-allodynia in male rats ($38.6 \pm 3\%$ for 1 $\text{mg}\cdot\text{kg}^{-1}$, $59 \pm 7\%$ for 3 $\text{mg}\cdot\text{kg}^{-1}$, $n = 10$ animals for both groups), but anti-allodynia was greatest for 10 $\text{mg}\cdot\text{kg}^{-1}$ Z944, indicating that this was

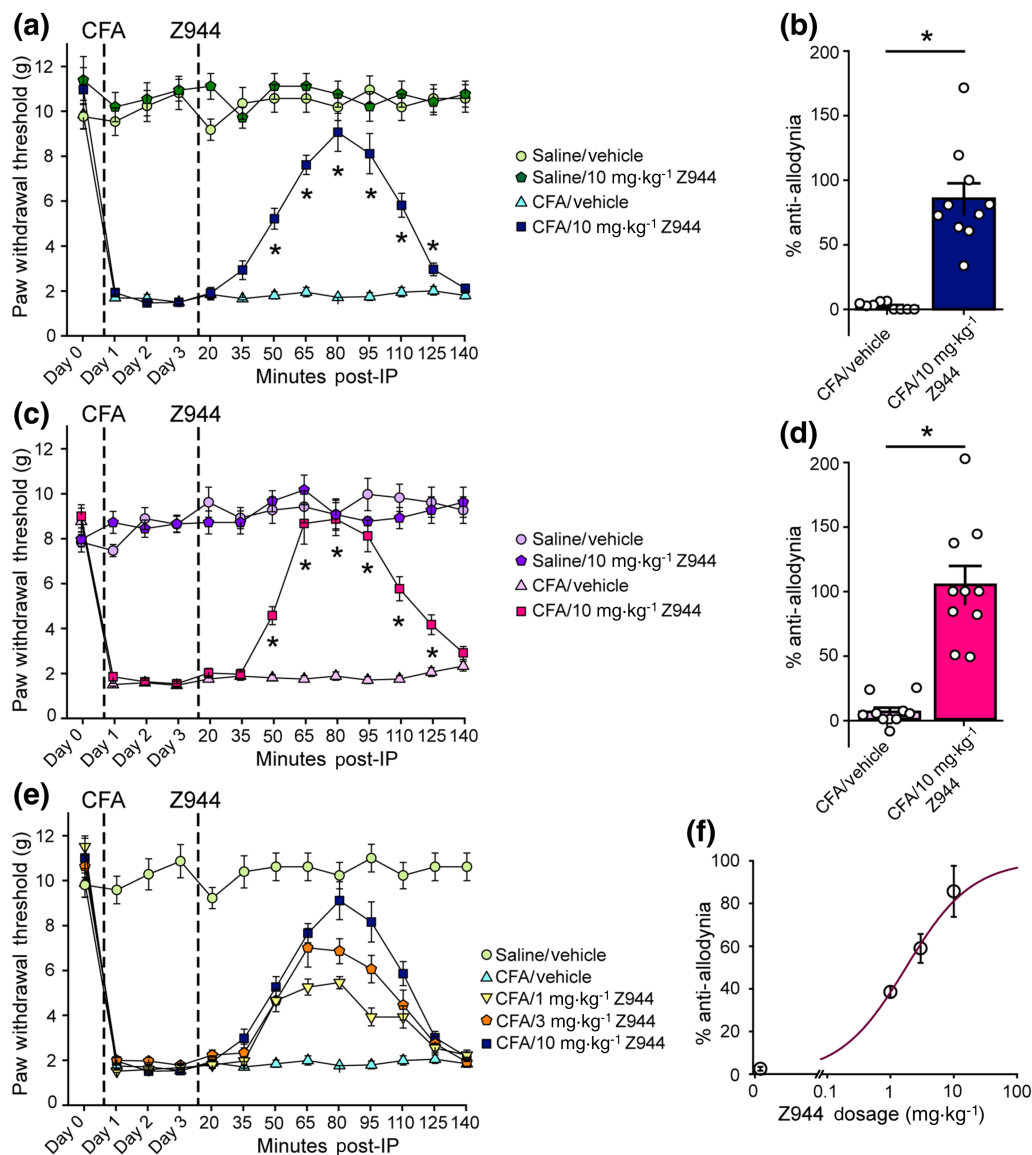


FIGURE 4 Intrapertoneal injection of Z944 reverses CFA-mediated tactile allodynia in both sexes, in a dose-dependent manner. (a) Paw withdrawal threshold, in grams, of adult male SD rats before (Day 0) and 1, 2, and 3 days following a hindpaw injection of either saline or CFA. Timepoints 20–140 min are following an i.p. injection of either 10 mg·kg⁻¹ Z944 or vehicle 3 days post-CFA injection ($n = 9$ animals for saline/vehicle and CFA/vehicle; $n = 10$ for saline/ mg·kg⁻¹ Z944 and CFA/10 mg·kg⁻¹ Z944). The effect of Z944 on CFA-induced tactile allodynia (dark blue) was determined with a one-way repeated measures ANOVA ($P < .05$), with Bonferroni post hoc comparisons to the Day 3 post-CFA injection baseline paw withdrawal threshold. (b) Percent anti-allodynia resulting from injection of either vehicle or 10 mg·kg⁻¹ Z944 in CFA injected male SD rats ($p = 4.9 \times 10^{-6}$, Mann-Whitney unpaired t -test, $n = 9$ animals for vehicle and 10 animals for Z944). Measures taken 80 min post-i.p. injection. (c) Paw withdrawal threshold, in grams, of adult female SD rats before (Day 0) and 1, 2, and 3 days following hindpaw injection of either saline or CFA. Timepoints 20–140 min are following i.p. injection of either 10 mg·kg⁻¹ Z944 or vehicle 3 days post-CFA injection ($n = 10$ animals for all groups). The effect of Z944 on CFA-induced tactile allodynia (dark pink) was determined with a one-way repeated measures ANOVA ($P < .05$), with Bonferroni post hoc comparisons to the Day 3 post-CFA injection paw withdrawal threshold. (d) Percent anti-allodynia resulting from injection of either vehicle or 10 mg·kg⁻¹ Z944 in CFA injected female SD rats ($p = 3.6 \times 10^{-6}$, Mann-Whitney unpaired t -test, $n = 10$ animals for vehicle, 10 animals for Z944). Measures taken 80 min post-i.p. injection. (e) Paw withdrawal threshold, in grams, of adult male SD rats before (Day 0) and 1, 2, and 3 days following a hindpaw injection of either saline or CFA. Timepoints 20–140 min are following i.p. injection of either 1, 3, or 10 mg·kg⁻¹ Z944 or vehicle 3 days post-CFA injection ($n = 10$ animals for all groups). (f) Percent anti-allodynia resulting from injection of either vehicle (0 mg·kg⁻¹ Z944) or 1, 3 or 10 mg·kg⁻¹ Z944 in CFA injected male SD rats. Measures taken 80 min post-i.p. injection. All error bars represent mean \pm SEM. * $P < .05$ for all post hoc comparisons

the most efficacious dose examined (Figure 4e). We found that anti-allodynia could be fit to a sigmoidal curve and obtained an IC_{50} of 1.76 ± 0.14 mg·kg⁻¹ for the anti-allodynic effects of Z944 (Figure 4f).

Taken together, our results suggest that Z944 potently reverses tactile allodynia produced by persistent inflammation in a dose-dependent manner, across both sexes.

4 | DISCUSSION

T-type calcium channels play a critical role in regulating neuronal excitability, but their role in lamina I pain processing neurons remains unclear. Furthermore, the role of T-type channels in mediating inflammatory pain across sexes has yet to be explored. Here, we used a combination of electrophysiology, calcium imaging and an *in vivo* CFA-induced inflammatory pain model in male and female rats to investigate the contributions of T-type calcium channels to pain signalling within lamina I neurons, including assessment of the effects of a selective T-type antagonist under clinical development, Z944, on lamina I neuronal excitability and CFA-mediated pain hypersensitivity.

4.1 | T-type channels are present in a large majority of lamina I neurons

We first sought to define the presence of T-type channels in lamina I neurons of adult rats. Voltage-clamp recordings of visually identified lamina I neurons demonstrated a fast inactivating inward current beginning at -60 mV in over 80% of neurons, indicating the presence of low voltage-activated currents most likely mediated by some combination of the three isoforms of T-type channels ($Ca_v3.1$, 3.2 , and 3.3) (Weiss & Zamponi, 2019). Although we saw a bias towards neurons with T-type channels being of the fusiform morphology, our preliminary results could not determine if there is a significant morphological difference in neurons with and without T-type channels, which could be used to infer population-type differences. Future studies could investigate this further by looking at the differential expression and function of T-type channel isoforms in genetically defined populations of lamina I neurons (Häring et al., 2018; Sathyamurthy et al., 2018).

In pharmacological experiments, we found that Z944 administration blocked over 50% of inward current at -60 and -50 mV within 5 min of perfusion, with no effect on inward current at 0 mV, demonstrating specificity to low voltage-activated T-type currents. These experiments provide compelling evidence for functional T-type channels in the majority of lamina I neurons. With a greater percentage of lamina I neurons (80%) containing T-type currents compared with lamina II (45 to 60%) (Candelas et al., 2019; Wu et al., 2018), these calcium channel variants may have a more prominent role in regulating the excitability of this critical subpopulation of nociceptive superficial dorsal horn neurons. Given that the $Ca_v3.2$ isoform of T-type channel regulates peripheral pain processing (Bourinet et al., 2014; Todorovic & Jevtovic-Todorovic, 2011; Weiss & Zamponi, 2019), is preferentially expressed in the superficial dorsal horn of the spinal cord (Li et al., 2017), and has recently been shown to control the excitability of lamina II spinal neurons (Candelas et al., 2019), it will also be important to investigate whether specific inhibition of post-synaptic $Ca_v3.2$ channels in the spinal cord mediates robust analgesia.

4.2 | Inhibition of T-type channels in lamina I neurons reduces action potential-induced calcium transients

Having demonstrated the presence of T-type channels in lamina I neurons, we next investigated how these channels contribute to neuronal excitability. Performing simultaneous two-photon calcium imaging while driving action potential firing in lamina I neurons showed that T-type channels contribute to over 50% of the action potential-evoked calcium response in both the soma and dendrites. In these experiments, since we were in current-clamp configuration we could not determine which neurons had a low voltage-activated component and therefore included all neurons for analysis, regardless of effect size. However, there was a high degree of variability in the percent peak remaining after the addition of Z944, ranging from 4% to 78% within the soma, and 13% to 67% within the dendrites. This heterogeneity in Z944 effect size raises the possibility that one or more neurons within this population may not have a substantial T-type component, after accounting for rundown present within the DMSO control. It is therefore likely that the true T-type contribution to action potential-evoked calcium responses is even larger in lamina I neurons containing T-type channels.

Our results indicate that T-type calcium channels are the predominant mediators of action potential-evoked calcium signals that, as we have previously demonstrated, represent actively backpropagating action potentials (Harding et al., 2020). Actively backpropagating action potentials shape the excitability of a neuron and have effects on both short-term and long-term plasticity. Dendritic T-type channels can drive LTP and LTD at specific hippocampal synapses (Udakis et al., 2020) and have also been shown to regulate dendritic excitability in cerebellar Purkinje neurons (Hildebrand et al., 2009) as well as in thalamocortical and thalamic reticular neurons (Connelly et al., 2015). Here, we have presented the first evidence that T-type channels are significant contributors to dendritic calcium transients in spinal lamina I neurons, suggesting that the use of Z944 could reduce the excitability of lamina I neurons and decrease the likelihood of these neurons to undergo activity-dependent synaptic plasticity (Frick et al., 2004; Rosenkranz et al., 2009; Short et al., 2017). Our results therefore have wide implications for the understanding of spinal mechanisms of pain processing and amplification. Further studies using pharmacological inhibitors of the other voltage-gated calcium channel classes are needed to systematically investigate the relative contribution of T-type versus high voltage-activated calcium channel classes in mediating these action potential-induced calcium responses in lamina I dendrites, as well as a potential role of dendritic T-type channels in governing lamina I neuron activity-dependent plasticity.

4.3 | Z944 reduces superficial dorsal horn neuron excitability

To directly examine the effect of Z944 on superficial dorsal horn neuron membrane excitability, we measured changes in rheobase in

recordings from a mixed population of lamina I and II neurons. In other neuron types, T-type channels contribute to membrane excitability and can promote burst firing through depolarizing the resting membrane potential, thus decreasing the current injection required to reach and sustain action potential threshold (Cain & Snutch, 2010). Here, we found that over half of superficial dorsal horn neurons responded to Z944 with a significant reduction in action potential firing in response to depolarization, suggesting that T-type channels also contribute to membrane excitability within the superficial dorsal horn, including both lamina I and II neurons.

Together, the above experiments indicate that administration of Z944 decreases the excitability of superficial dorsal horn neurons, providing a novel, central mechanism through which T-type channel blockers may also exert their analgesic effects. These findings are of particular significance in light of recent findings demonstrating that the peripherally restricted T-type antagonist ABT-639 fails to show efficacy in clinical trials for pain (Serra et al., 2015; Wallace et al., 2016). This suggests that inhibition of T-type channels by Z944 in the superficial dorsal horn may hold future promise for effective clinical application.

4.4 | Z944 as a potential treatment for inflammatory pain

Although previous studies have found that T-type antagonists can produce analgesia, these studies have relied on T-type channel blockers with significantly less selectivity, such as ethosuximide, [mibefradil](#) and NiCl_2 , raising the possibility of action through inhibition of other ion channels such as high voltage-activated calcium channels and voltage-gated sodium channels (Dogrul et al., 2003; Feng et al., 2019; Flatters & Bennett, 2004). In contrast, Z944 is a high affinity T-type channel antagonist, with no significant block of high voltage-activated calcium channels or sodium channels at concentrations sufficient to block T-type channels (Tringham et al., 2012) and has been shown to be well tolerated in human clinical trials (Lee, 2014). We found that i.p. injection of Z944 produced a profound reversal of CFA-induced tactile allodynia in both male and female rats, in a clear dose-dependent manner without affecting baseline mechanical sensitivity. Z944 was well tolerated over a large therapeutic window with an IC_{50} of $1.76 \pm 0.14 \text{ mg}\cdot\text{kg}^{-1}$. We are the first to demonstrate that Z944 reverses mechanical allodynia in both sexes, which is an important step in preclinical investigation.

T-type calcium channels are also expressed in peripheral DRG sensory neurons, presynaptic terminals of nociceptive primary afferents, and higher order brain structures involved in nociceptive processing (Bourinet et al., 2014; Jacus et al., 2012; Leblanc et al., 2016). As i.p. injection of Z944 induces systemic exposure of Z944 to both the peripheral nervous system and CNS, the analgesic efficacy of Z944 in reversing CFA-induced pain hypersensitivity could also be due to inhibition of T-type channels at these additional nociceptive loci. To directly confirm that Z944 exerts analgesic effects through acting on spinal cord T-type channels, pain thresholds and

behaviours could be assessed after intrathecal injection of Z944 in rodent models of chronic pain. In combination with the above suggested knockdown of T-type isoforms in dorsal horn neuron subpopulations, this future work would shed further light on spinal cord T-type channels as a specific target for the development of novel pain therapeutics.

In summary, we have identified low threshold calcium currents as well as somatic and dendritic calcium transients that are mediated by T-type channels in lamina I neurons of the spinal dorsal horn, which are effectively inhibited by the administration of the highly selective T-type channel blocker Z944. Moreover, we have demonstrated that Z944 potently reverses tactile allodynia produced by persistent inflammation in a dose-dependent manner, across both sexes. Together, our findings indicate that the anti-allodynic effect of T-type channel block may be through inhibition of superficial dorsal horn neuron excitability, in addition to the previously defined peripheral mechanisms, implying a central mechanism for Z944's analgesic actions.

ACKNOWLEDGMENTS

MH was supported by an Industrial R&D Fellowship and a Discovery Grant (CU#315915) from the Natural Sciences and Engineering Research Council of Canada for the superficial dorsal horn electrophysiology (Figure 3) and behavioural (Figure 4) experiments in this study, respectively. Work in the laboratory of TPS was supported by a grant from the Canadian Institutes of Health Research Institute of Neurosciences, Mental Health and Addiction (10677). Work in the laboratory of MWS was supported by a grant from the Canadian Institutes of Health Research Institute of Neurosciences, Mental Health and Addiction (154336). We thank Dr. Chris Rudyk, Rikesh Raichura, and Chris Dedek for preparing injections and blinding for i.p. injections.

AUTHOR CONTRIBUTIONS

All authors contributed to experimental design. E.K.H., A.D. and M.E.H. performed the experiments and analyses. All authors contributed to manuscript preparation.

CONFLICT OF INTEREST

The authors have declared that no conflict of interest exists.

DECLARATION OF TRANSPARENCY AND SCIENTIFIC RIGOUR

This Declaration acknowledges that this paper adheres to the principles for transparent reporting and scientific rigour of preclinical research as stated in the *BJP* guidelines for [Design and Analysis](#) and [Animal Experimentation](#), and as recommended by funding agencies, publishers and other organisations engaged with supporting research.

DATA AVAILABILITY STATEMENT

The data that support the findings of this study are available from the corresponding author upon reasonable request.

ORCID

Erika K. Harding  <https://orcid.org/0000-0003-3941-3411>
 Annemarie Dedek  <https://orcid.org/0000-0002-7215-4928>
 Robert P. Bonin  <https://orcid.org/0000-0002-3287-6803>
 Michael W. Salter  <https://orcid.org/0000-0001-6897-6585>
 Terrance P. Snutch  <https://orcid.org/0000-0001-5182-1296>
 Michael E. Hildebrand  <https://orcid.org/0000-0002-6845-8013>

REFERENCES

- Alexander, S. P. H., Mathie, A., Peters, J. A., Veale, E. A., Striessnig, J., Kelly, E., Armstrong, J. F., Faccenda, E., Harding, S. D., Pawson, A. J., Sharman, J. L., Southan, C., Davies, J. A., & CGTP Collaborators. (2019). the Concise Guide to PHARMACOLOGY 2019/20: Ion channels. *BJP*, 176(S1), S142–S228.
- Bonin R. P., Bories C., De Koninck Y. (2014). A simplified up-down method (SUDO) for measuring mechanical nociception in rodents using von Frey filaments. *Molecular Pain*, 10(26), 1744–8069. <https://doi.org/10.1186/1744-8069-10-26>
- Bourinet, E., Alloui, A., Monteil, A., Barrère, C., Couette, B., Poirot, O., Pages, A., McRory, J., Snutch, T. P., Eschalièr, A., & Nargeot, J. (2005). Silencing of the Cav3.2 T-type calcium channel gene in sensory neurons demonstrates its major role in nociception. *The EMBO Journal*, 24, 315–324. <https://doi.org/10.1038/sj.emboj.7600515>
- Bourinet, E., Altier, C., Hildebrand, M. E., Trang, T., Salter, M. W., & Zamponi, G. W. (2014). Calcium-permeable ion channels in pain signaling. *Physiological Reviews*, 94, 81–140. <https://doi.org/10.1152/physrev.00023.2013>
- Cain, S. M., & Snutch, T. P. (2010). Contributions of T-type calcium channel isoforms to neuronal firing. *Channels*, 4, 475–482. <https://doi.org/10.4161/chan.4.6.14106>
- Cain, S. M., & Snutch, T. P. (2013). T-type calcium channels in burst-firing, network synchrony, and epilepsy. *Biochimica et Biophysica Acta, Biomembranes*, 1828, 1572–1578. <https://doi.org/10.1016/j.bbmem.2012.07.028>
- Cain, S. M., Tyson, J. R., Choi, H.-B., Ko, R., Lin, P. J. C., LeDue, J. M., Powell, K. L., Bernier, L. P., Rungta, R. L., Yang, Y., Cullis, P. R., O'Brien, T. J., MacVicar, B. A., & Snutch, T. P. (2018). Ca_v 3.2 drives sustained burst-firing, which is critical for absence seizure propagation in reticular thalamic neurons. *Epilepsia*, 59, 778–791. <https://doi.org/10.1111/epi.14018>
- Candelas M., Reynders A., Arango-Lievano M., Neumayer C., Fruquière A., Demes E., Hamid J., Lemmers C., Bernat C., Monteil A., Compan V., Laffray S., Inquimbert P., Le Feuvre Y., Zamponi G. W., Moqrich A., Bourinet E., Méry P.-F. (2019). Cav3.2 T-type calcium channels shape electrical firing in mouse Lamina II neurons. *Scientific Reports*, 9, (1–18). <http://dx.doi.org/10.1038/s41598-019-39703-3>.
- Casillas-Espinosa, P. M., Shultz, S. R., Braine, E. L., Jones, N. C., Snutch, T. P., Powell, K. L., & O'Brien, T. J. (2019). Disease-modifying effects of a novel T-type calcium channel antagonist, Z944, in a model of temporal lobe epilepsy. *Progress in Neurobiology*, 182, 101677. <https://doi.org/10.1016/j.pneurobio.2019.101677>
- Cheong, E., & Shin, H.-S. (2013). T-type Ca²⁺ channels in normal and abnormal brain functions. *Physiological Reviews*, 93, 961–992. <https://doi.org/10.1152/physrev.00010.2012>
- Connelly, W. M., Crunelli, V., & Errington, A. C. (2015). The global spike: Conserved dendritic properties enable unique Ca²⁺ spike generation in low-threshold spiking neurons. *The Journal of Neuroscience*, 35, 15505–15522. <https://doi.org/10.1523/JNEUROSCI.2740-15.2015>
- Curtis, M. J., Alexander, S., Cirino, G., Docherty, J. R., George, C. H., Giembycz, M. A., Hoyer, D., Insel, P. A., Izzo, A. A., Ji, Y., MacEwan, D. J., Sobey, C. G., Stanford, S. C., Teixeira, M. M., Wonnacott, S., & Ahluwalia, A. (2018). Experimental design and analysis and their reporting II: Updated and simplified guidance for authors and peer reviewers. *British Journal of Pharmacology*, 175, 987–993. <https://doi.org/10.1111/bph.14153>
- Dedek, A., Xu, J., Kandedgedara, C. M., Lorenzo, L.-É., Godin, A. G., De Koninck, Y., Lombroso, P. J., Tsai, E. C., & Hildebrand, M. E. (2019). Loss of STEP61 couples disinhibition to N-methyl-D-aspartate receptor potentiation in rodent and human spinal pain processing. *Brain*, 142, 1535–1546. <https://doi.org/10.1093/brain/awz105>
- Dogrul, A., Gardell, L. R., Ossipov, M. H., Tulunay, F. C., Lai, J., & Porreca, F. (2003). Reversal of experimental neuropathic pain by T-type calcium channel blockers. *Pain*, 105, 159–168. [https://doi.org/10.1016/S0304-3959\(03\)00177-5](https://doi.org/10.1016/S0304-3959(03)00177-5)
- Feng, X. J., Ma, L. X., Jiao, C., Kuang, H. X., Zeng, F., Zhou, X. Y., Cheng, X. E., Zhu, M. Y., Zhang, D. Y., Jiang, C. Y., & Liu, T. (2019). Nerve injury elevates functional Cav3.2 channels in superficial spinal dorsal horn. *Molecular Pain*, 15, 1744806919836569.
- Flatters, S. J. L., & Bennett, G. J. (2004). Ethosuximide reverses paclitaxel- and vincristine-induced painful peripheral neuropathy. *Pain*, 109, 150–161. <https://doi.org/10.1016/j.pain.2004.01.029>
- François, A., Schüetter, N., Laffray, S., Sanguesa, J., Pizzoccaro, A., Dubel, S., Mantilleri, A., Nargeot, J., Noël, J., Wood, J. N., Moqrich, A., Pongs, O., & Bourinet, E. (2015). The low-threshold calcium channel Cav3.2 determines low-threshold mechanoreceptor function. *Cell Reports*, 10, 370–382. <https://doi.org/10.1016/j.celrep.2014.12.042>
- Frick, A., Magee, J., & Johnston, D. (2004). LTP is accompanied by an enhanced local excitability of pyramidal neuron dendrites. *Nature Neuroscience*, 7, 126–135. <https://doi.org/10.1038/nn1178>
- Fukami, K., Sekiguchi, F., & Kawabata, A. (2017). Hydrogen sulfide and T-type Ca²⁺ channels in pain processing, neuronal differentiation and neuroendocrine secretion. *Pharmacology*, 99, 196–203. <https://doi.org/10.1159/000449449>
- García-Caballero, A., Gadotti, V. M., Stemkowski, P., Weiss, N., Souza, I. A., Hodgkinson, V., Bladen, C., Chen, L., Hamid, J., Pizzoccaro, A., Deage, M., François, A., Bourinet, E., & Zamponi, G. W. (2014). The deubiquitinating enzyme USP5 modulates neuropathic and inflammatory pain by enhancing Cav3.2 channel activity. *Neuron*, 83, 1144–1158. <https://doi.org/10.1016/j.neuron.2014.07.036>
- Gomez, K., Calderón-Rivera, A., Sandoval, A., González-Ramírez, R., Vargas-Parada, A., Ojeda-Alonso, J., Granados-Soto, V., Delgado-Lezama, R., & Felix, R. (2020). Cdk5-dependent phosphorylation of Ca_v3.2 T-type channels: Possible role in nerve ligation-induced neuropathic allodynia and the compound action potential in primary afferent C fibers. *The Journal of Neuroscience*, 40, 283–296. <https://doi.org/10.1523/JNEUROSCI.0181-19.2019>
- Harding, E. K., Boivin, B., & Salter, M. W. (2020). Intracellular calcium responses encode action potential firing in spinal cord lamina I neurons. *The Journal of Neuroscience*, 40, 4439–4456. <https://doi.org/10.1523/JNEUROSCI.0206-20.2020>
- Häring, M., Zeisel, A., Hochgerner, H., Rinwa, P., Jakobsson, J. E. T., Lönnerberg, P., la Manno, G., Sharma, N., Borgius, L., Kiehn, O., Lagerström, M. C., Linnarsson, S., & Ernfors, P. (2018). Neuronal atlas of the dorsal horn defines its architecture and links sensory input to transcriptional cell types. *Nature Neuroscience*, 21, 869–880. <https://doi.org/10.1038/s41593-018-0141-1>
- Hildebrand, M. E., Isope, P., Miyazaki, T., Nakaya, T., Garcia, E., Feltz, A., Schneider, T., Hescheler, J., Kano, M., Sakimura, K., Watanabe, M., Dieudonne, S., & Snutch, T. P. (2009). Functional coupling between mGluR1 and Cav3.1 T-type calcium channels contributes to parallel fiber-induced fast calcium signaling within Purkinje cell dendritic spines. *The Journal of Neuroscience*, 29, 9668–9682. <https://doi.org/10.1523/JNEUROSCI.0362-09.2009>
- Hildebrand, M. E., Pitcher, G. M., Harding, E. K., Li, H., Beggs, S., & Salter, M. W. (2014). GluN2B and GluN2D NMDARs dominate synaptic responses in the adult spinal cord. *Scientific Reports*, 4, 4094

- Hildebrand M. E., Smith P. L., Bladen C., Eduljee C., Xie J. Y., Chen L., Fee-Maki M., Doering C. J., Mezeyova J., Zhu Y., Belardetti F., Pajouhesh H., Parker D., Arneric S. P., Parmar M., Porreca F., Tringham E., Zamponi G. W., Snutch T. P. (2011). A novel slow-inactivation-specific ion channel modulator attenuates neuropathic pain. *Pain*, 152, (4), 833–843. <http://dx.doi.org/10.1016/j.pain.2010.12.035>.
- Ikeda, H., Heinke, B., Ruscheweyh, R., & Sandkühler, J. (2003). Synaptic plasticity in spinal lamina I projection neurons that mediate hyperalgesia. *Science*, 299, 1237–1240. <https://doi.org/10.1126/science.1080659>
- Jacus, M. O., Uebele, V. N., Renger, J. J., & Todorovic, S. M. (2012). Presynaptic Cav3.2 channels regulate excitatory neurotransmission in nociceptive dorsal horn neurons. *The Journal of Neuroscience*, 32, 9374–9382. <https://doi.org/10.1523/JNEUROSCI.0068-12.2012>
- Joksimovic, S. L., Joksimovic, S. M., Manzella, F. M., Asnake, B., Orestes, P., Raol, Y. H., Krishnan, K., Covey, D. F., Jevtovic-Todorovic, V., & Todorovic, S. M. (2019). Novel neuroactive steroid with hypnotic and T-type calcium channel blocking properties exerts effective analgesia in a rodent model of post-surgical pain. *British Journal of Pharmacology*, 177, 1735–1753. <https://doi.org/10.1111/bph.14930>
- Keller, A. F., Beggs, S., Salter, M. W., & De Koninck, Y. (2007). Transformation of the output of spinal lamina I neurons after nerve injury and microglia stimulation underlying neuropathic pain. *Molecular Pain*, 3, 1744–8069–3–27.
- Kuo, A., Wyse, B. D., Meuterms, W., & Smith, M. T. (2015). In vivo profiling of seven common opioids for antinociception, constipation and respiratory depression: No two opioids have the same profile. *British Journal of Pharmacology*, 172, 532–548. <https://doi.org/10.1111/bph.12696>
- Leblanc, B. W., Li, T. R., Huang, J. J., Chao, Y. C., Bowary, P. M., Cross, B. S., Lee, M. S., Vera-Portocarrero, L. P., & Saab, C. Y. (2016). T-type calcium channel blocker Z944 restores cortical synchrony and thalamocortical connectivity in a rat model of neuropathic pain. *Pain*, 157, 255–263. <https://doi.org/10.1097/j.pain.0000000000000362>
- Lee, M. (2014). Z944: A first in class T-type calcium channel modulator for the treatment of pain. In *Journal of the Peripheral Nervous System* (pp. S11–S12). Blackwell Publishing Inc.
- Li, Y., Tatsui, C. E., Rhines, L. D., North, R. Y., Harrison, D. S., Cassidy, R. M., Johansson, C. A., Kosturakis, A. K., Edwards, D. D., Zhang, H., & Dougherty, P. M. (2017). Dorsal root ganglion neurons become hyperexcitable and increase expression of voltage-gated T-type calcium channels (Cav3.2) in paclitaxel-induced peripheral neuropathy. *Pain*, 158, 417–429. <https://doi.org/10.1097/j.pain.0000000000000774>
- Lilley E., Stanford S. C., Kendall D. E., Alexander S. P. H., Cirino G., Docherty J. R., George C. H., Insel P. A., Izzo A. A., Ji Y., Panettieri R. A., Sobey C. G., Stefanska B., Stephens G., Teixeira M., Ahluwalia A. (2020). ARRIVE 2.0 and the British Journal of Pharmacology: Updated guidance for 2020. *British Journal of Pharmacology*, 177, (16), 3611–3616. <http://dx.doi.org/10.1111/bph.15178>.
- Lima, D., & Coimbra, A. (1986). A Golgi study of the neuronal population of the marginal zone (lamina I) of the rat spinal cord. *The Journal of Comparative Neurology*, 244, 53–71. <https://doi.org/10.1002/cne.902440105>
- Liu, X. J., Gingrich, J. R., Vargas-Caballero, M., Dong, Y. N., Sengar, A., Beggs, S., Wang, S. H., Ding, H. K., Frankland, P. W., & Salter, M. W. (2008). Treatment of inflammatory and neuropathic pain by uncoupling Src from the NMDA receptor complex. *Nature Medicine*, 14, 1325–1332. <https://doi.org/10.1038/nm.1883>
- Mogil, J. S. (2012). Sex differences in pain and pain inhibition: Multiple explanations of a controversial phenomenon. *Nature Reviews. Neuroscience*, 13, 859–866. <https://doi.org/10.1038/nrn3360>
- Percie du Sert, N., Hurst, V., Ahluwalia, A., Alam, S., Avey, M. T., Baker, M., Browne, W. J., Clark, A., Cuthill, I. C., Dirnagl, U., Emerson, M., Garner, P., Holgate, S. T., Howells, D. W., Karp, N. A., Lazic, S. E., Lidster, K., MacCallum, C. J., Macleod, M., ... Würbel, H. (2020). The ARRIVE guidelines 2.0: Updated guidelines for reporting animal research. *PLoS Biology*, 18(7), e3000410. <https://doi.org/10.1371/journal.pbio.3000410>
- Picard, E., Carvalho, F. A., Agosti, F., Bourinet, E., Ardid, D., Eschaliere, A., Daulhac, L., & Mallet, C. (2019). Inhibition of Ca_v 3.2 calcium channels: A new target for colonic hypersensitivity associated with low-grade inflammation. *British Journal of Pharmacology*, 176, 950–963. <https://doi.org/10.1111/bph.14608>
- Ren, K., Hylden, J. L., Williams, G. M., Ruda, M. A., & Dubner, R. (1992). The effects of a non-competitive NMDA receptor antagonist, MK-801, on behavioral hyperalgesia and dorsal horn neuronal activity in rats with unilateral inflammation. *Pain*, 50, 331–344. [https://doi.org/10.1016/0304-3959\(92\)90039-E](https://doi.org/10.1016/0304-3959(92)90039-E)
- Rosenkranz, J. A., Frick, A., & Johnston, D. (2009). Kinase-dependent modification of dendritic excitability after long-term potentiation. *The Journal of Physiology*, 587, 115–125. <https://doi.org/10.1113/jphysiol.2008.158816>
- Sathyamurthy, A., Johnson, K. R., Matson, K. J. E., Dobrott, C. I., Li, L., Ryba, A. R., Bergman, T. B., Kelly, M. C., Kelley, M. W., & Levine, A. J. (2018). Massively parallel single nucleus transcriptional profiling defines spinal cord neurons and their activity during behavior. *Cell Reports*, 22, 2216–2225. <https://doi.org/10.1016/j.celrep.2018.02.003>
- Serra, J., Duan, W. R., Locke, C., Solà, R., Liu, W., & Nothaft, W. (2015). Effects of a T-type calcium channel blocker, ABT-639, on spontaneous activity in C-nociceptors in patients with painful diabetic neuropathy. *Pain*, 156, 2175–2183. <https://doi.org/10.1097/j.pain.0000000000000249>
- Short, S. M., Oikonomou, K. D., Zhou, W.-L., Acker, C. D., Popovic, M. A., Zecevic, D., & Antic, S. D. (2017). The stochastic nature of action potential backpropagation in apical tuft dendrites. *Journal of Neurophysiology*, 118, 1394–1414. <https://doi.org/10.1152/jn.00800.2016>
- Sorge, R. E., Mapplebeck, J. C. S., Rosen, S., Beggs, S., Taves, S., Alexander, J. K., Martin, L. J., Austin, J. S., Sotocinal, S. G., Chen, D., Yang, M., Shi, X. Q., Huang, H., Pillon, N. J., Bilan, P. J., Tu, Y. S., Klip, A., Ji, R. R., Zhang, J., ... Mogil, J. S. (2015). Different immune cells mediate mechanical pain hypersensitivity in male and female mice. *Nature Neuroscience*, 18, 1081–1083. <https://doi.org/10.1038/nn.4053>
- Todd, A. J. (2010). Neuronal circuitry for pain processing in the dorsal horn. *Nature Reviews. Neuroscience*, 11, 823–836. <https://doi.org/10.1038/nrn2947>
- Todorovic, S. M., & Jevtovic-Todorovic, V. (2011). T-type voltage-gated calcium channels as targets for the development of novel pain therapies. *British Journal of Pharmacology*, 163, 484–495. <https://doi.org/10.1111/j.1476-5381.2011.01256.x>
- Tringham, E., Powell, K. L., Cain, S. M., Kuplast, K., Mezeyova, J., Weerapura, M., Eduljee, C., Jiang, X., Smith, P., Morrison, J. L., & Jones, N. C. (2012). T-type calcium channel blockers that attenuate thalamic burst firing and suppress absence seizures. *Science Translational Medicine*, 4, 121ra19.
- Tsubota, M., Okawa, Y., Irie, Y., Maeda, M., Ozaki, T., Sekiguchi, F., Ishikura, H., & Kawabata, A. (2018). Involvement of the cystathionine- γ -lyase/Cav3.2 pathway in substance P-induced bladder pain in the mouse, a model for nonulcerative bladder pain syndrome. *Neuropharmacology*, 133, 254–263. <https://doi.org/10.1016/j.neuropharm.2018.01.037>
- Udakis M., Pedrosa V., Chamberlain S. E. L., Clopath C., Mellor J. R. (2020). Interneuron-specific plasticity at parvalbumin and somatostatin inhibitory synapses onto CA1 pyramidal neurons shapes hippocampal output. *Nature Communications*, 11, (1–17). <http://dx.doi.org/10.1038/s41467-020-18074-8>.

- Wallace, M., Duan, R., Liu, W., Locke, C., & Nothaft, W. (2016). A randomized, double-blind, placebo-controlled, crossover study of the T-type calcium channel blocker ABT-639 in an intradermal capsaicin experimental pain model in healthy adults. *Pain Medicine*, *17*, 551–560. <https://doi.org/10.1093/pm/pnv068>
- Watanabe, M., Ueda, T., Shibata, Y., Kumamoto, N., Shimada, S., & Ugawa, S. (2015). Expression and regulation of Cav3.2 T-type calcium channels during inflammatory hyperalgesia in mouse dorsal root ganglion neurons. *PLoS ONE*, *10*, e0127572.
- Wei, F., Vadakkan, K. I., Toyoda, H., Wu, L. J., Zhao, M. G., Xu, H., Shum, F. W., Jia, Y. H., & Zhuo, M. (2006). Calcium calmodulin-stimulated adenylyl cyclases contribute to activation of extracellular signal-regulated kinase in spinal dorsal horn neurons in adult rats and mice. *The Journal of Neuroscience*, *26*, 851–861. <https://doi.org/10.1523/JNEUROSCI.3292-05.2006>
- Weiss, N., & Zamponi, G. W. (2019). T-type calcium channels: From molecule to therapeutic opportunities. *The International Journal of Biochemistry & Cell Biology*, *108*, 34–39. <https://doi.org/10.1016/j.biocel.2019.01.008>
- Wen, X.-J., Xu, S.-Y., Chen, Z.-X., Yang, C.-X., Liang, H., & Li, H. (2010). The roles of T-type calcium channel in the development of neuropathic pain following chronic compression of rat dorsal root ganglia. *Pharmacology*, *85*, 295–300. <https://doi.org/10.1159/000276981>
- Wu, J., Peng, S., Xiao, L., Cheng, X., Kuang, H., Zhu, M., Zhang, D., Jiang, C., & Liu, T. (2018). Cell-type specific distribution of T-type calcium currents in lamina II neurons of the rat spinal cord. *Frontiers in Cellular Neuroscience*, *12*, 370–13. <https://doi.org/10.3389/fncel.2018.00370>
- Zhao, Y., Huang, G., Wu, Q., Wu, K., Li, R., Lei, J., Pan, X., & Yan, N. (2019). Cryo-EM structures of apo and antagonist-bound human Cav3.1. *Nature*, *576*, 492–497. <https://doi.org/10.1038/s41586-019-1801-3>

SUPPORTING INFORMATION

Additional supporting information may be found online in the Supporting Information section at the end of this article.

How to cite this article: Harding EK, Dedek A, Bonin RP, Salter MW, Snutch TP, Hildebrand ME. The T-type calcium channel antagonist, Z944, reduces spinal excitability and pain hypersensitivity. *Br J Pharmacol*. 2021;178:3517–3532. <https://doi.org/10.1111/bph.15498>